ChemComm

COMMUNICATION

View Article Online
View Journal

CrossMark click for updates

Cite this: DOI: 10.1039/c5cc00926j

Received 31st January 2015,
Accepted 3rd March 2015

DOI: 10.1039/c5cc00926j

www.rsc.org/chemcomm

Published on 03 March 2015. Downloaded on 17/03/2015 11:39:12.

Electrocatalytic water oxidation by Cu^{II} complexes with branched peptides†

József S. Pap,*[a] Łukasz Szyrwiel,*[bc] Dávid Srankó,[a] Zsolt Kerner,[a] Bartosz Setner,[d] Zbigniew Szewczuk[d] and Wiesław Malinka[b]

Two mononuclear Cu^{II} complexes with tetrapeptides incorporating a L-2,3-diaminopropionic acid (dap) branching unit are reported to undergo PCET and catalyse water oxidation. C-terminal His extension of dap (L = 2GH) instead of Gly (L = 3G) lowers the pK_a for $Cu^{III}H_{-2}L$ (9.36 *vs.* 9.98) and improves the TOF at pH 11 (53 *vs.* 24 s^{-1}).

Reactions requiring the synchronous transfer of multiple protons and electrons become energetically viable under mild conditions through the catalytic promotion of proton-coupled electron transfer (PCET) mechanisms that help circumventing high-energy intermediates.[1] Splitting water into its elements, which attracts growing attention as a prospective renewable tool to generate H_2 as an energy carrier,[2–4] ranks among reactions where PCET is of critical importance. Water oxidation catalysts (WOCs) can improve the efficiency of the oxidative half-reaction: $2H_2O \rightarrow O_2 + 4H^+ + 4e^-$, which has long been considered the bottleneck of the water splitting process. Bioinspired, homogeneous WOCs (Fe,[5] Co,[6] Ru,[7] or Ir [8]), although inherently less robust than heterogeneous catalysts,[9] represent a meaningful source of mechanistic insight into the multiple proton and electron-transfer events associated with O_2 formation. A growing number of studies conclude that PCET helps in stabilising high-valent M=O or M–O$^\bullet$ intermediates by preventing charge accumulation upon oxidation and, as a consequence these intermediates can complete the O–O bond formation step.[10] Cu has rich oxygen chemistry,[11] yet, homogeneous WOCs involving this metal appeared only recently, when surprisingly robust Cu^{II} complexes with 2,2′-bipyridine (bpy, TOF ~ 100 s^{-1} at pH 13)[12] and subsequently, with triglycylglycine (GGGG, or H-Gly-Gly-Gly-Gly-OH, TOF = 33 s^{-1} at pH 11, Scheme 1)[13] were reported as water oxidation electrocatalysts. Modification of $Cu^{II}(bpy)(OH)_2$ by using 6,6′-dihydroxy-bpy demonstrated the potential of tuning such systems toward better efficiency (*e.g.*, reduced overpotential) by aiding proton channelling.[14] The modularity of peptides opens even more options to affect the catalytic properties from the ligand side. Experimental information is presented below in support of water oxidation electrocatalysis at elevated pH in the presence of Cu complexes with two different dap-based peptides: H-Gly-Dap(H-Gly)-Gly-NH_2 (3G) and H-Gly-Dap(H-Gly)-His-NH_2 (2GH) (Scheme 1). These peptides were reported to form stable 1 : 1 Cu^{II} complexes that are distinguished by their ligand set and stability at basic pH resulting from the equatorially coordinated C-terminal His residue in 2GH.[15]

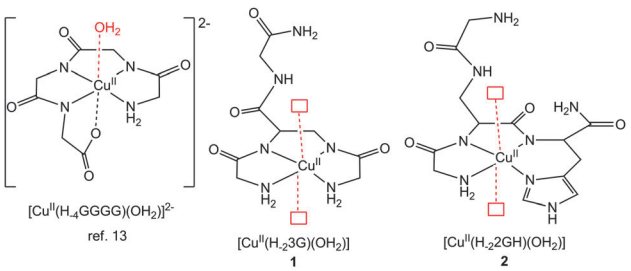

Scheme 1 View of the dominant forms of Cu–peptide complexes at basic pH. Red squares represent available sites for H_2O coordination as the fifth ligand.

According to potentiometry, the predominant form of the 1 : 1 Cu^{II} complex above pH 7 (L = 3G) or above pH 8 (L = 2GH) is $Cu^{II}H_{-2}L$ (**1** and **2**, respectively) alike. Parallel X-Band EPR, UV/VIS and CD spectroscopic changes with increasing pH suggested a $\{NH_2,2N^-,NH_2\}$ equatorial ligand set for **1**.[15] Based on analogous examples,[13,16] a further deprotonation step resulting in $Cu^{II}H_{-3}L$ (**1**–H^+) in the case of **1** has been associated with proton loss from an axially coordinated water molecule. In **2**, Cu^{II} is bound by a $\{NH_2,2N^-,N_{Im}\}$ equatorial set, involving the C-terminal histidine residue. A similar 5,5,6 chelate pattern was also suggested for the Cu^{II} complex of the linear H-Gly-Gly-His-OH.[17] No further deprotonation of **2** was detected in potentiometry up to pH 11.

[a] Centre for Energy Research, Surface Chemistry and Catalysis Department, P.O. Box 49, H-1525 Budapest 114, Hungary. E-mail: pap.jozsef@energia.mta.hu
[b] Department of Chemistry of Drugs, Wrocław Medical University, ul. Borowska 211, 50-552 Wrocław, Poland. E-mail: lukasz.szyrwiel@umed.wroc.pl
[c] CNRS/UPPA, LCABIE, UMR5254, Helioparc, 2, av. Pr. Angot, F-64053 Pau, France
[d] Faculty of Chemistry, University of Wrocław, ul. F. Joliot-Curie 14, 50–383 Wrocław, Poland

† Electronic supplementary information (ESI) available: Experimental, Fig. S1–S12, Tables S1–S3. See DOI: 10.1039/c5cc00926j

Published on 03 March 2015. Downloaded on 17/03/2015 11:39:12.

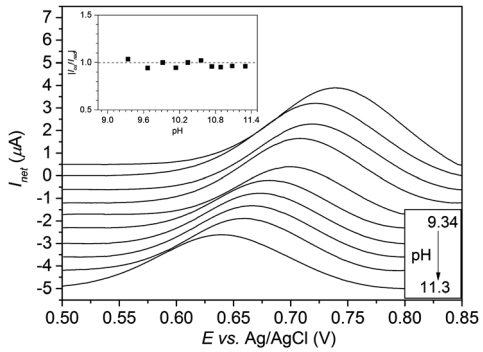

Fig. 1 Variation of SWV response with pH in a Cu : 2GH = 0.9 : 1 solution. Conditions: [Cu] = 0.2 mM, 0.1 M $NaClO_4$, pH set with NaOH, 25 °C, under Ar, P_H = 25 mV, f = 12.5 Hz, S_H = 0.2 mV. The inset shows the $|I_{for}/I_{net}|$ ratio. Concomitant voltammograms are shifted by ~5 mV for better visuals.

Cu–peptides bearing a 4N donor set are known for allowing reversible $Cu^{III/II}$ redox couples at potentials inversely related to the number of deprotonated amidic N donors of the order of: $\{NH_2,3N^-\}$ (0.41 V *vs.* Ag/AgCl)[18] < $\{N_{Im},3N^-\}$ (0.66 V *vs.* Ag/AgCl)[19] < $\{N_{Im},NH_2,2N^-\}$ (0.77 V *vs.* Ag/AgCl).[20] Electrochemical characterization of **1** and **2** was carried out by square-wave voltammetry (SWV, see ESI† for experimental). In Fig. 1 SWV plots are shown as a function of pH for **2** (for **1** see Fig. S1, ESI,† for data see Tables S1 and S2, ESI†). The E_{net}[21] observed by $|I_{for}/I_{net}|$ of *ca.* 1 (a landmark for reversibility, see inset of Fig. 1 and Fig. S1, ESI†) can be directly associated with the formal potential for the $Cu^{III/II}$ oxidation.[22,23]

In Fig. 2 the E_{net} ($\sim E^{\circ\prime}$) data points are plotted against pH generating a Pourbaix diagram for the $Cu^{III/II}$ process of **1** and **2**. The inverse variation of the potential with pH suggests PCET; however, nonlinearity indicates equilibrium species in different protonation states that affect $E^{\circ\prime}$.

If we suppose that the PCET process is described by eqn (1),

$$\begin{array}{lcl} Cu^{III}H_{-3}L + e^- + H^+ & \rightleftharpoons & Cu^{II}H_{-2}L \\ \mathbf{1^{ox}} - H^+, \text{ if } L = 3G & & \mathbf{1} \\ \mathbf{2^{ox}} - H^+, \text{ if } L = 2GH & & \mathbf{2} \end{array} \quad (1)$$

where $Cu^{III}H_{-3}L$ corresponds to a Cu^{III}–OH species, the modified Nernst equations, eqn (2) and (3), explain the Pourbaix diagrams.[24]

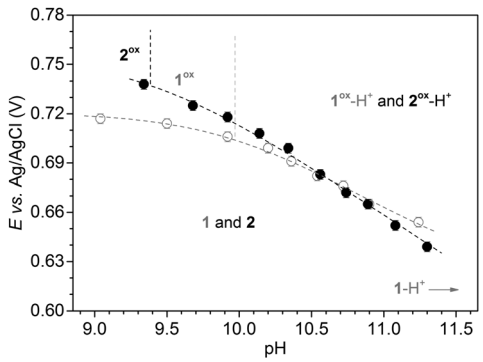

Fig. 2 $Cu^{III/II}$ E_{net} ($E^{\circ\prime}$) values plotted against pH (**1**: open circles, **2**: black circles). Dashed curves represent a nonlinear regression fit to eqn (2), R^2 = 0.996 and (3), R^2 = 0.994, vertical lines denote pK_{ox} values. $pK_{red/ox}$ and $E^{\circ\prime}$ values from best fit are listed in Table 1.

In eqn (2) one equilibrium is considered both for $\mathbf{1^{ox}}$ (K_{ox}) and **1** (K_{red}), while in eqn (3), only one equilibrium for $\mathbf{2^{ox}}$ (K_{ox}):

$$E_{net}(\mathbf{1}) = E^{\circ\prime}(\mathbf{1^{ox}} - H^+, H^+/\mathbf{1}, pH = 0) + 0.0591 \log\frac{K_{red}K_{ox} + K_{ox}[H^+]}{K_{ox} + [H^+]} \quad (2)$$

$$E_{net}(\mathbf{2}) = E^{\circ\prime}(\mathbf{2^{ox}} - H^+, H^+/\mathbf{2}, pH = 0) + 0.0591 \log\frac{K_{ox}[H^+]}{K_{ox} + [H^+]} \quad (3)$$

where K_{red} is the acid dissociation constant of **1** to **1**–H^+, K_{ox} is that for $\mathbf{1^{ox}}$ and $\mathbf{2^{ox}}$ to $\mathbf{1^{ox}}$–H^+ and $\mathbf{2^{ox}}$–H^+, respectively, $E^{\circ\prime}$($\mathbf{1^{ox}}$–H^+,H^+/**1**, pH = 0) and $E^{\circ\prime}$($\mathbf{2^{ox}}$–H^+,H^+/**2**, pH = 0) denote the formal potentials of the process in eqn (1). Fit of eqn (2) and (3) to the corresponding E_{net} data points yields the dashed lines in Fig. 2 and parameters as listed in Table 1.

The $E^{\circ\prime}$($\mathbf{1^{ox}}$/**1**) (0.72 V *vs.* Ag/AgCl) and $E^{\circ\prime}$($\mathbf{2^{ox}}$/**2**) (0.76 V *vs.* Ag/AgCl) values can also be deduced from the fittings and compared to examples with a reported equatorial binding plane.[13,18–20] The high values and the $E^{\circ\prime}$($\mathbf{1^{ox}}$/**1**) < $E^{\circ\prime}$($\mathbf{2^{ox}}$/**2**) relationship are in accordance with the suggested $\{NH_2,2N^-,NH_2\}$ and $\{NH_2,2N^-,N_{Im}\}$ donor planes, respectively. The presence of **1**–H^+ (*e.g.*, Cu^{II}–OH) is in line with potentiometry.[15,25]

Cyclic voltammetry (CV) was performed on **1** and **2** in phosphate buffer (PB) at a glassy carbon working electrode (GCE). Upon increasing the pH to 11, a new electrocatalytic wave occurs (Fig. S2, ESI†) with an onset potential over 1.0 V *vs.* Ag/AgCl, similar to what was associated with water oxidation catalysis by $[Cu^{II}(H_{-4}GGGG)(OH_2)]^{2-}$.[13] The E_{cat} peak potential varies inversely with pH and the I_{cat} peak current becomes substantially larger. The possibility of a deposition process or decomposition of the complex was ruled out by using freshly polished GCE and successive cycling experiments (Fig. S3, ESI†). Dioxygen evolution was confirmed over multiple cycles under Ar by detecting the O_2 reduction wave[6,10,12] and comparing it with the corresponding wave under air (Fig. S4, ESI†). The catalytic current changes linearly with the concentration of **1** and **2** (Fig. 3, Table S3, ESI†), when scanned at 5 mV s^{-1}, but drastically drops at higher scan rates (ν) (Fig. S5 and S6, ESI†) indicating that the rate determining step (r.d.s.) is a chemical process involving one complex molecule. Diffusion coefficients for the complexes among catalytic conditions were determined from the Randles–Sevcik equation (see Fig. S7, ESI†), and thus TOFs (k_{cat}) of 24 and 53 s^{-1} could be calculated from the catalyst dependence plots (see Fig. 3 inset).[26]

Controlled potential electrolysis (CPE) was performed at 1.1 V *vs.* Ag/AgCl with an indium-tin-oxide working electrode (ITO) in a 0.5 mM solution of **2**. The concentration of O_2 grew instantly at

Table 1 Formal potentials and $pK_{red/ox}$ values derived from the fit of eqn (2) and (3) to experimental E_{net} *vs.* pH data for the $Cu^{III/II}$ redox transition

	eqn (2)	eqn (3)
pK_{red}	11.7 ± 0.2	
$E^{\circ\prime}$ *vs.* Ag/AgCl (V)	1.311 ± 0.002	1.309 ± 0.001
pK_{ox}	9.98 ± 0.05	9.36 ± 0.07

 This journal is © The Royal Society of Chemistry 2015

Published on 03 March 2015. Downloaded on 17/03/2015 11:39:12.

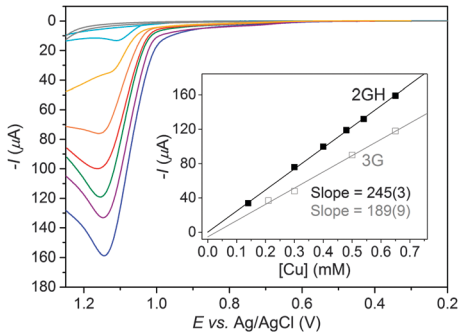

Fig. 3 Effect of complex concentration (**2**) on I_{cat} (pH 11, 0.15 M PB, 25 °C, ν = 5 mV s^{-1}, no catalyst – grey, 0.5 mM $CuSO_4$ – light blue). Inset: $-I_{cat}$ *vs.* [Cu] plots for **1** (grey) and **2** (black). TOF values were calculated from slopes as given.[26]

the start of CPE (Fig. S8, ESI†). X-Ray photoelectron spectroscopy (XPS) on ITO before and after CPE (Fig. S9, ESI†) evidenced no Cu deposition (Fig. S10 and S11, ESI†), and transferring the rinsed ITO to a fresh PB produced no O_2 during CPE.[27] Our observations imply that the catalyst is of molecular nature (note that the role of a supported or colloidal material cannot be ruled out completely) and the introduction of a C-terminal His promotes catalysis in conjunction with the acidity of coordinated water in $\mathbf{2^{ox}}$.

Meyer proposed a mechanism for the Cu–peptide catalyst that starts with the $[Cu^{II}–OH_2]^{2-} \rightarrow [Cu^{III}–OH]^{2-} \rightarrow [Cu^{III}–O^{\bullet}]^{2-}$ oxidation sequence *via* PCET reactions, and yields intermediate Cu^{II}–peroxide by the reaction of $[Cu^{III}–O^{\bullet}]^{2-}$ with H_2O in a r.d.s. Catalytic enhancement and irreversibility of the second anodic wave were proposed to come from further oxidation of the peroxide, release of O_2 and re-entry into the catalytic cycle.[13] Our very similar observations (PCET furnishing $\mathbf{1^{ox}}(\mathbf{2^{ox}})$–$H^+$ and a linear change in I_{cat} with [Cu]) suggest that the catalytically enhanced wave (E_{cat}) following the $Cu^{III/II}$ transition of **1**(**2**) ($E^{\circ\prime}$) should come from the oxidation of $\mathbf{1^{ox}}(\mathbf{2^{ox}})$–$H^+$ to $[(H_{-2}L)Cu^{III}–O^{\bullet}]$ that forms intermediate Cu^{II}–peroxide with H_2O in a r.d.s. Further steps can be figured analogous to Meyer's mechanism (Scheme S1, ESI†). In this case the His in **2** can facilitate PCET reactions in the course of catalysis, possibly by means of π-interaction with protons (Scheme S1 caption, ESI†) explaining the higher TOF and lower pK_{ox} for $\mathbf{2^{ox}}$. Surface anchoring of the complexes and synthesis of catalytic dendrimers based on dap are among future plans.

This work was supported by MTA (János Bolyai Research Scholarship to J. S. Pap) and by Polish Foundation of Science within the POMOST program co-financed by the EU within European Regional Development Fund (POMOST/2012-5/9).

Notes and references

1 D. R. Weinberg, C. J. Gagliardi, J. F. Hull, C. F. Murphy, C. A. Kent, B. C. Westlake, A. Paul, D. H. Ess, D. G. McCafferty and T. J. Meyer, *Chem. Rev.*, 2012, **112**, 4016.
2 T. R. Crook, D. K. Dogutan, S. Y. Reece, Y. Surendranath, T. S. Teets and D. G. Nocera, *Chem. Rev.*, 2010, **110**, 6474.
3 *Solar hydrogen generation – toward a renewable energy future*, ed. K. Rajeshwar, R. McConnel and S. Licht, Springer, New York, NY, 2008.
4 N. S. Lewis and D. G. Nocera, *Proc. Natl. Acad. Sci. U. S. A.*, 2006, **103**, 15729.
5 J. L. Fillol, Z. Codola, I. Garcia-Bosch, L. Gomez, J. J. Pla and M. Costas, *Nat. Chem.*, 2011, **3**, 807.
6 D. J. Wasylenko, C. Ganesamoorthy, J. Borau-Garcia and C. P. Berlinguette, *Chem. Commun.*, 2011, **47**, 4249.
7 L. Duan, F. Bozoglian, S. Mandal, B. Stewart, T. Privalov, A. Llobet and L. Sun, *Nat. Chem.*, 2012, **4**, 418.
8 J. D. Blakemore, N. D. Schley, D. Balcells, J. F. Hull, G. W. Olack, C. D. Incarvito, O. Eisenstein, G. W. Brudvig and R. H. Crabtree, *J. Am. Chem. Soc.*, 2011, **132**, 16017.
9 V. Artero and M. Fontecave, *Chem. Soc. Rev.*, 2013, **42**, 2338.
10 M. D. Kärkäs, O. Verho, E. V. Johnston and B. Akermark, *Chem. Rev.*, 2014, **114**, 11863.
11 *Copper-Oxygen Chemistry*, ed. K. D. Karlin and S. Itoh, John Wiley & Sons, Inc., Hoboken, New Jersey, 2011.
12 S. M. Barnett, K. I. Goldberg and J. M. Mayer, *Nat. Chem.*, 2012, **4**, 498.
13 M.-T. Zhang, Z. Chen, P. Kang and T. J. Meyer, *J. Am. Chem. Soc.*, 2013, **135**, 2048.
14 T. Zhang, C. Wang, S. Liu, J.-L. Wang and W. Lin, *J. Am. Chem. Soc.*, 2014, **136**, 273.
15 Ł. Szyrwiel, Ł. Szczukowski, J. S. Pap, B. Setner, Z. Szewczuk and Z. Malinka, *Inorg. Chem.*, 2014, **53**, 7951.
16 L. M. P. Lima, D. Esteban-Gómez, R. Delgado, C. Platas-Iglesias and R. Tripier, *Inorg. Chem.*, 2012, **51**, 6916.
17 N. I. Jakab, B. Gyurcsik, T. Körtvélyesi, I. Vosekalna, J. Jensen and E. Larsen, *J. Inorg. Biochem.*, 2007, **101**, 1376.
18 D. W. Margerum, K. L. Chellappa, F. P. Bossu and G. L. Burce, *J. Am. Chem. Soc.*, 1975, **97**, 6874.
19 C. Hureau, L. Charlet, P. Dorlet, F. Gonnet, L. Spadini, E. Anxolabéhére-Mallart and J.-J. Girerd, *JBIC, J. Biol. Inorg. Chem.*, 2006, **11**, 735.
20 C. Hureau, H. Eury, R. Guillot, C. Bijani, S. Sayen, P.-L. Solari, E. Guillon, P. Faller and P. Dorlet, *Chem. – Eur. J.*, 2011, **17**, 10151.
21 Where I_{net}, the difference in the forward and reverse current upon opposite polarization pulse, *e.g.*, $I_{for} - I_{rev} = I_{net}$, reaches maximum.
22 *Electroanalytical Methods*, ed. F. Scholz, Springer-Verlag, Berlin, 2010.
23 B. W. Berry, M. C. Martínez-Rivera and C. Tommos, *Proc. Natl. Acad. Sci. U. S. A.*, 2010, **109**, 9739.
24 P. Wardman, *J. Phys. Chem. Ref. Data*, 1989, **18**, 1637.
25 Inclusion of K_{red} in eqn (2) results in a significantly better fit to the data; however, its value being outside of the investigated pH range makes any quantitative conclusions elusive.
26 The TOF (k_{cat}) values were determined from the slope of linears fitted to $-I_{cat}$ *vs.* [Cu] data points shown in Fig. 3 inset, by applying equation: I_{cat} (μA) = $n_{cat}FA$[Cu]$(k_{cat}D_{Cu})^{0.5}$, where n_{cat} = 4, F is the Faraday constant, A = 0.071 cm^2, [Cu] is the concentration of **1** or **2** (mM), and D_{Cu} is the diffusion coefficient of the complex in 0.15 M PB at pH 11, that is 2 × 10^{-6} cm^2 s^{-1} for **1** and 1.5 × 10^{-6} cm^2 s^{-1} for **2**.
27 Tests were run using suspensions made with $CuSO_4$ or $Cu(ClO_4)_2$ at pH 11, since Cu salts were reported to generate catalytic thin films at pH 10.8 (Z. Chen and T. J. Meyer, *Angew. Chem., Int. Ed.*, 2013, **52**, 700). A substantial deposit consisting of CuO and $Cu(OH)_2$ was detected on ITO (Fig. S12, ESI†), a feature missing from ITOs used in complex solutions (Fig. S11, ESI†). After over 90 min of CPE, the amount of O_2 detected by a fluorescent probe corresponded to TONs of 6.3 for **2** and 5.1 for **1**, with Faradaic efficiency (*e.g.*, 100 × (det./theor. O_2)%) of 91% and 95%, respectively. CPE was performed in 0.5 mM solutions (6 mL) of **1** and **2** at 25 °C, under air. The electric charges (Q) were 8.20 and 6.56 C, equivalent to 16 and 21.2 μmol O_2 (Q/4F). Detected O_2 was 15.3 and 19.3 μmol, respectively. The UV/VIS spectra before and after electrolysis showed ∼25% (**1**, λ_{max} = 527 nm) and ∼30% (**2**, λ_{max} = 530 nm) decrease in absorbance.